BJMG 28 (2), 2025 • 29-40
DOI: 10.2478/bjmg-2025-00024

ORIGINAL ARTICLE

IDENTIFICATION OF A NOVEL HOMOZYGOUS *IHH* VARIANT CAUSING NOVEL ACROMESOMELIC MAROTEAUX-TYPE SKELETAL DYSPLASIA IN A PAKISTANI FAMILY

Hanif M[1], Ahmad B[1], Farman S[1], Hassan S[2], Hayat A[1], Bibi N[3], Kalsoom U[4], Khan B[1]

[*]**Corresponding Author:** Bushra Khan PhD, Department of Biochemistry, Faculty of Life and Chemical Sciences, Abdul Wali khan University, Mardan, KP, Pakistan; Tel: +923335274595, E-mail: bushrakhan@awkum.edu.pk; ID 0000-0002-3239-496X

ABSTRACT

Acromesomelic dysplasias (AMDs) are rare skeletal disorders marked by disproportionate shortening of middle and distal limb segments. Among these, AMD Maroteaux type (AMDM), is commonly associated with mutations in *NPR2* gene. However, mutations in the Indian Hedgehog *(IHH)* gene have been linked to several skeletal dysplasia with overlapping features. In the present study, we report a consanguineous Pakistani family presenting with a novel AMDM type skeletal dysplasia that phenotypically resembles but is distinct from AMDM. Mmutational screening was carried out by whole exome sequencing (WES) followed by Sanger sequencing. In silico modeling and molecular dynamics simulation analysis were used to validate the variant. WES identified a novel homozygous missense variant in the *IHH* gene (c.1018G>A; p. Val340Met) which segregated within the family and was absent in unaffected ethnically matched controls. Structural modelling and simulations indicated that the p. Val340Met substitution destabilizes the IHH C-terminal auto processing domain leading to reduced compactness and stability. These changes are predicted to impair IHH processing and function, thereby contributing to disease onset. This study reports a novel form of AMDM type skeletal dysplasia in a Pakistani family, and identify the novel homozygous *IHH* variant, thereby expanding the phenotypic and mutational spectrum of *IHH*-related skeletal disorders.

Keywords: Acromesomelic Maroteaux type, autosomal recessive, homozygous missense variant, *IHH* gene

INTRODUCTION

Acromesomelic dysplasia (AMD) comprise of a group of progressive skeletal disorders marked by dwarfism associated with anomalies affecting both the middle (mesomelic) and distal (acromelic) portions of the limbs. AMD can occur in both syndromic and isolated (non-syndromic) forms. The syndromic form is often associated with additional abnormalities involving the genital, respiratory, cardiac and neurological systems [1-2]. These disorders are subclassified based on clinical features and underlying genetic mutations. The latest revision of nosology included 7 different kinds of AMD [3-4]. Autosomal recessive forms of AMDs include: AMD1(OMIM #602875); AMD-2A (OMIM #200700), AMD-2B (OMIM #228900), and AMD-2C (OMIM #201250); AMD3 (OMIM #200700) and AMD4 (OMIM #619636). An autosomal dominant form of acromesomelic dysplasia Osebold-Remondini type (OMIM #112910) has also been reported with an unidentified causative gene [5-11].

Acromesomelic dysplasia type Maroteaux (AMDM/ AMD1) is caused by mutations in the *NPR2* (natriuretic peptide receptor B) gene on chromosome 9p13–q12. It is diagnosed at birth or becomes apparent by infancy and is presented with short stature, bowed forearms, short metacarpals and phalanges, broad tibiae and fibulae, ankle deformities, coxa valga and cortical thickening [12-14]. In comparison AMD type 2 variants (AMD2A–C) which are

[1] Department of Biochemistry, Abdul Wali Khan University, Mardan, KPK, Pakistan: hanifawkum85@gmail.com; bakhan009@gmail.com; sairafarman@awkum.edu.pk; aamir.hayatqau15@gmail.com

[2] Department of Biochemistry, institute of Basic Medical Sciences, Khyber Medical University Peshawar, Pakistan: Salmanhassan.ibms@kmu.edu.pk

[3] Shaheed Benazir Bhutto Women University, Peshawar, Pakistan: drnosheenbibi@sbbwu.edu.pk

[4] Department of Biochemistry, Hazara University, Mansera, Pakistan: kalsoom_ibrahim@hotmail.com; kalsoom.u@hu.edu.pk

caused by the mutations in the GDF6 gene (chromosome 20q11) primarily affects the limbs with a proximal-to-distal severity gradient: Grebe type (AMD2A) shows the most severe involvement with non-articulated, rudimentary digits[15]; Du Pan type (AMD2B) is characterized by fibular hypoplasia or absence with severe hand and foot anomalies[7]; and Hunter–Thompson type (AMD2C) with limb-restricted abnormalities, relatively preserved distal phalanges, and variable joint dislocations while craniofacial and axial structures remain normal across all types[15].

Another rare form of acromesomelic dysplasia is Acrocapitofemoral dysplasia (ACFD OMIM #607778) characterized clinically by short stature with short limbs, narrow thorax, relatively large head, brachydactyly with small broad nails and lumbar lordosis. Radiographically it is manifested by egg-shaped femoral head connected to markedly short femoral neck with a small collar-like bony outgrowth and cone-shaped epiphyses predominantly affecting hands and hips [16-17]. Homozygous missense mutations in the Indian Hedgehog (*IHH)* gene have been reported to cause ACFD [18-19]. On the other hand, heterozygous dominant variants in *IHH* have been reported to be involved in brachydactyly type A1 (BDA1) (OMIM #112500). BDA1 is defined by shortening of the phalanges or metacarpals, most notably the middle phalanges, particularly those of 2nd and 5th digits—along with distal or terminal symphalangism that varies with disease severity. This condition also involves shortening of the thumb's proximal phalanges, as well as the metacarpals and metatarsals. BDA1 patients often have a short stature (dwarfism) [20].

Mutation underlying both ACFD and BDA1 are restricted to the amino-terminal functional domain of *IHH* gene [17-19]. However, in a study by [21], ten heterozygous IHH variants in 17 families with autosomal dominant short stature were identified. Interestingly these families did not study show classic features of BDA1 and the identified variants were dispersed throughout the gene. This suggests that the phenotypic spectrum of IHH-associated disorders is broader than previously recognized, with clinical severity influenced by the variant's location, functional impact, and inheritance pattern.

In the present study, we present a novel report of a homozygous missense variant (c.1018G>A, p. Val340Met) in the carboxy terminal region of the *IHH* gene in a consanguineous Pakistani family affected with Acromesomelic Maretoux-type like skeletal dysplasia. The affected individuals exhibited disproportionate short stature, mesomelic and acromelic limb shortening, Madelung deformity, brachydactyly, clinodactyly, coxa vara, genu varum, hip dysplasia and bilateral foot deformity (fixed equinus). These features, together with the genetic evidence, support the involvement of the *IHH* gene in a novel form of autosomal recessive acromesomelic skeletal dysplasia.

MATERIALS AND METHODS

Sample collection and Whole Exome Sequencing

Family was recruited and samples obtained with informed written consent under a protocol approved by the Institutional Ethical Review Board of the Abdul Wali Khan University Mardan (Pakistan). A four-generation pedigree was constructed after consultation with family elders (Figure 1a). Affected members (IV-1, IV-3, IV-4) underwent clinical examination at local government hospitals. The extraction of Genomic DNA was performed using standard methods (Sambrook et al. 1989). Whole-exome sequencing (WES) was performed using the Illumina HiSeq: Agilent Sureselect Whole Exome v6 targeting was used for exome capture, read alignment was done using BWA-MEM (v0.7.17) which was followed by mate-pairs fixed and duplicates removal by Picard v2.15.0 was used, followed by InDel realignment and base quality recalibration with GATK v3.7.0, and subsequent detection of single-nucleotide variants (SNVs) and InDel by GATK Haplotype Caller, and annotation by Alamut v1.8. Sequencing depth was assessed with GATK DepthOfCoverage. Based on the most likely inheritance pattern inferred from pedigree analysis, homozygous, compound heterozygous, and heterozygous variants were prioritized. Selection criteria included a minor allele frequency ≤ 0.005 in gnomAD, a CADD-Phred score ≥ 15, exonic or splice-site variants (± 12 bp), and phenotypic similarity of candidate genes to the family phenotype. Segregation of selected variants was confirmed by Sanger sequencing in all available family members. PCR primers were designed using the Primer3 tool (https://primer3.ut.ee) while the reference gene sequences were retrieved from the UCSC Genome Browser (https://genome.ucsc.edu/).

3D structure modelling

I-Tasser server was used to build three-dimensional structure of human HH C-terminal auto-processing domain of wildtype IHH protein (IHH^{WT}) through homology modelling approach [22] using 1at.0 PDB molecule as template with 36.36% identity. Next, Insilco mutagenesis approach mutant three-dimensional structure of IHH($IHH^{Val340Met}$) protein was built through I-Tasser server [22] using IHH^{WT} protein model as template. Predicted model were refined by WinCoot [23]and stereochemistry and validity of constructed 3D structure of human IHH^{WT} protein (C-terminal auto-processing domain) and mutant $HH^{Val340Met}$ was assessed by Ramachandran plot [24] PROCHECK [25] and verify 3D [26]. To measure the effect of identified mutation on protein structure HOPE server [27] was used.

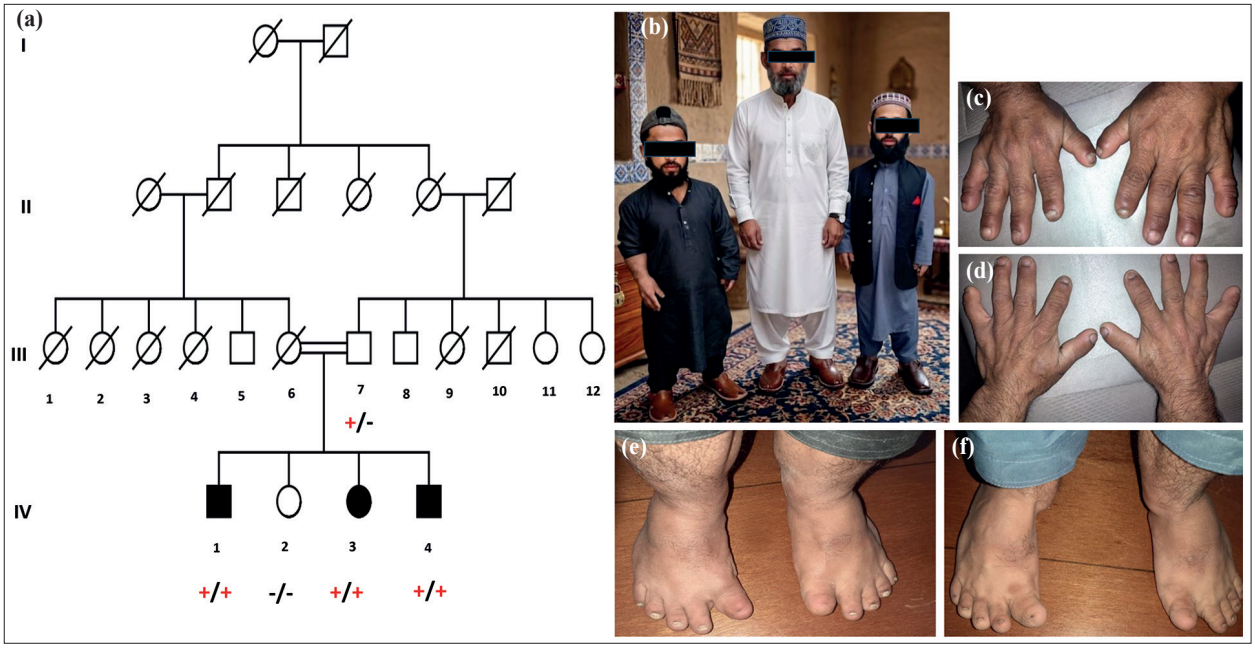

Figure 1. (a) Pedigree of family exhibiting autosomal recessive pattern. (b) The father (III-7), of average height along with the affected males (IV-4, IV-1) who are short statured with normal trunk length and markedly shortened arms and legs. (c, d) Hands of affected males (IV-1 and IV-4) are short and broad. Clinodactyly is seen. Nails are dystrophic, with irregular curvature and thickening. (e, f) Clinical Photographs of feet of IV-1and IV-4 demonstrate broad, flat feet with disproportionately short and stubby toes. Toenails are dystrophic, with bilateral hyponychia of the great toes.

Molecular dynamic simulations

Comparative MD simulations of IHH^{WT} and $IHH^{Val-340Met}$ (c-terminal auto processing domain) were performed to evaluate the conformational alterations, stability, and dynamic properties of the IHH protein. GROMACS 4.5 package was used to do simulations experiments by using Amber03 force field [28]and solvated using the TIP4P water model [29] within a periodic box. Next, Na^+ and Cl^- counter ions were added to both (IHH^{WT} and $IHH^{Val340Met}$) systems to neutralize them. Simulations were carried out for a duration of 20ns time scale under constant conditions of temperature (300K) and pressure (1 atm) for the IHH^{WT} and $IHH^{Val340Met}$ systems. The stability of the secondary structure elements stability along with their interactions and conformational changes were assessed using UCSF Chimera.

RESULTS

Clinical findings

The affected siblings, IV-1 (male, 28 years), IV-3 (female, 26 years), IV-4 (male 22 years) were born from a consanguineous union following full-term pregnancies without complications. At the time of evaluation IV-1 measured 116.84 cm in height (−9.6 SD), weighed 38.5 kg, hand length of 40.64cm and wrist-to-finger length of 15.24cm; IV-3 had a height of 99.06cm(-9.7 SD), weighed 32 kg, hand 38.1cm, wrist to fingers 15.24cm; IV-4 had a height of 121.92cm(−10.4 SD), weighed 38 kg, ,upper limb length (shoulder to fingertip) of 41.14cm and wrist to finger length of 15.66cm. Head circumference of the three affected (IV-1, IV-3, IV-4) was 54.61,50.8,53.84cm, respectively. Father of the affected individuals (55 years old) was of average height 160.02 cm (-1.54SD) and weight of 65 kg (Figure 1b). Head circumference and hand length were 54.61 cm and 66.04cm respectively. Based on the available information, the mother was reported to be clinically normal with no skeletal abnormalities. All the three affected individuals had very short stature with normal trunk length, severely shortened arms and legs (Figure 1b). Hands were short and broad. Fingers, especially the thumbs and index were short relative to the hand size. The 5th fingers on both hands showed inward deviation toward the 4th fingers. Nails appeared dystrophic, with irregular curvature and thickening (Figure 1c, d). Feet were broad and flat, with disproportionately short, broad, and stubby toes. Toes nails were dystrophic with bilateral hyponychia in big toes. Bowed legs (genu varum) were also evident in the standing image (Figure 1e, f) (Table 1).

Lateral and anterior posterior radiographs of the skull of the affected members (IV-1 and IV-4) showed normal craniofacial proportions but increased radiodensity of the calvarium. No midface hypoplasia and frontal bossing was observed (Figure 2a-d). The upper limb X-rays of the same individuals revealed mildly shortened humerus, bilateral

Table 1. Phenotypic comparison of the patients reported in the present family with AMDM, ACFD, AMD2A, AMD2B and AMD2C

Characteristics	Current Study IV-1	IV-3	IV-4	AMD1/ Maroteaux	ACFD	AMD2A / Grebe (GDF5)	AMD2B / Du Pan (GDF5)	AMD2C (GDF5)
Phenotypic Features								
Age (years)	26	28	22	NA	NA	NA	NA	NA
Height (cm ± SD)	116.84 cm (−9.6 SD)	99.06cm (-9.7 SD)	121.92cm (−10.4 SD)	<125 cm (−6 to −10 SD)	84, 102 cm (-2.3 to −9.6 SD)	~100 cm (severe)	Mild–moderate short stature	Severe short stature
Weight (kg)	38.5,	32.0	,38	Low	20–30	Low	Low	Low
Head Circumference (cm ± SD)	54.61	50.8	53.84	Macrocephaly	50.8–54.6	Normal	Normal	Normal
Acromesomelic Limb Shortening	✓	✓	✓	✓	✓	✓ (Severe Distal)	✓	✓
Head size	Near normal	Near normal	Near normal	Normal	Large	Normal	Normal	Normal
Intelligence	Normal	Normal	Normal	Normal	Normal	Normal	Normal	Normal
Brachydactyly	✓	✓	✓	✓	✓	✓ (Severe)	✓ (complex)	✓
Clinodactyly	✓	✓	✓	✓	✓	✓	✓	✓
Hyponychia	✓	✓	✓	×	×	×	✓	×
Loose redundant skin	×	×	×	✓	×	✓	✓	✓
Joint laxity	×	×	×	✓	×	×	×	✓
Feet deformity	Equinus deformity/ Metatarsus Adductus	Equinus deformity/ Metatarsus Adductus	Equinus deformity/ Metatarsus Adductus	Large halluces	Pes planus	Valgus foot deformity	Talipes equinovalgus	Short feet
Radiological Features								
Radial bowing & angulation	**Severe (Madelung-like)**	**Severe (Madelung-like)**	**Severe (Madelung-like)**	✓	Mild due to coning	×	×	×
Dislocated radial head	✓	✓	✓	Rare	Rare	✓	Occasional	occasional
Subluxation of ulnocarpal joint	✓	✓	✓	×	×	✓	✓	✓
Retarded/dislocated Carpal bone age	Marked Delay	Marked Delay	Marked Delay	Marked Delay	Moderate Delay	Extreme Delay/ Fused	Mild Delay/Fused (Rudimentary)	Mild Delay/Fused (Rudimentary)
Suprapatellar Loose Bodies	✓	×	×	×	×	×	×	×
Fusion of phalanges	Synostosis	Synostosis	Synostosis	×	Synostosis	Symphalangism	Symphalangism	×
Metacarpals	Short	Short	Short	Short	Teardrop	Rudimentary or absent metacarpals	Tear drop	Cuboidal/ Extremely short
Short phalanges	Proximal phalanges	Proximal phalanges	Proximal phalanges	Middle and proximal phalanges	Middle and Distal	Rudimentary (distal present only)	Middle and proximal	Middle and proximal
Thorax	Normal	Normal	Normal	Normal	Narrow	Normal	Normal	Normal
Vertebral changes	×	×	×	(kyphosis)	(lumbar lordosis)	×	×	×
Chest	Normal	Normal	Normal	Superiorly curved clavicles	Pectus deformities	Normal	Normal	Normal
Acetabulum	Normal	Normal	Normal	Dysplastic	Dysplastic	Dysplastic	Dysplastic	Dysplastic
Iliac Wings	Normal	Normal	Normal	Squared	Short	Hypoplastic	small	small
Coxa valga / vara	Vara	Vara	Vara	Valga	Vara	Dislocated	Valga	Valga
Cortical Thickness	Increased	Increased	Increased	Normal	Normal	Normal	Normal	Normal
Medullary canals	Narrow	Narrow	Narrow	Normal	Normal	Normal	Normal	Normal
Short tibia/fibula	✓	✓	✓	✓	✓	✓ (Severely shortened)	✓ (fibula absent/ hypoplastic)	✓
Metaphyseal Shape	Flared/Irregular	Flared/ Irregular	Flared/ Irregular	Severely Flared	V shaped	Rudimentary	Normal	Normal
Cone Shaped Epiphysis	×	×	×	×	✓	×	×	×
Short femoral neck/shaft	✓	✓	✓	✓	✓	✓	✓	✓
Distal femur	Hyper Plastic	Hyper Plastic	Hyper Plastic	Broad	Normal	Hypoplastic	Normal to broad	Normal
GenuValgum/Varum	Varum	Varum	Varum	×	Varum	Valgum	Valgum	Valgum
Autosomal Recessive Inheritance	✓	✓	✓	✓	✓	✓	✓	✓
Gene mutated	*IHH*	*IHH*	*IHH*	*NPR2*	*IHH*	*GDF5*	*GDF5*	*GDF5*

"✓" indicates presence and; "×" indicates absence: Abbreviations: SD, standard deviation.

shortened radius and ulna with thickened cortices and narrow medullary canals, more pronounced in the distal radius. There was also volar and ulnar bowing of the distal radius, along with dorsal subluxation of the distal ulna and increased radial inclination supporting the diagnosis of Madelung deformity (Figure 2e-h). Chest radiographs of the affected individual IV-1and IV-4 were normal while the chest and upper limb radiographs of the affected individual IV-3 showed Madelung deformity characterized by radial bowing with increased cortical density of the long bones, and normal thorax and vertebral column (Figure 2i-k). Radiographs of the hands of the individuals IV-1, IV-3 and IV-4 showed severe brachydactyly with generalized cortical sclerosis of the metacarpals and phalanges. The 4th and 5th metacarpals were disproportionately shortened and appeared stubbier compared to other metacarpals. The phalanges, particularly the proximal were mildly shortened with relatively preserved alignment and morphology. In addition, the carpal bones appeared to form a V-shaped (triangular) configuration at the proximal carpal row. No cone-shaped epiphyses, synostosis, or overt joint dislocations were identified in the visualized phalanges (Figure 2l-n). Pelvis radiographs of the affected individuals IV-1, IV-3 and IV-4 revealed short femoral necks with decreased neck-shaft angles consistent with coxa vara. The femoral shafts showed cortical thickening with narrowing of medullary canal. Hip and knee joint spaces were preserved (Figure 2o-q). Lower limb radiographs showed shortened and broad tibia and fibula with genu varum (bowing of the legs). There was flaring and irregularity of the metaphysis at the distal femora and proximal tibiae. The cortices appeared thickened, and the medullary canals were narrowed. Additionally

Figure 2. (a–d) Lateral and anteroposterior (AP) skull radiographs of affected individual IV-1 and IV-4 show generalized calvarial thickening with absence of frontal bossing and no evidence of macrocephaly. (e-h) Left and right upper limb radiograph of affected individuals (IV-1, IV-4) showing bilateral shortening of the radius and ulna, with cortical thickening and narrowed medullary canals, most pronounced in the distal radius. Features of true Madelung deformity, including volar-ulnar bowing of the distal radius, dorsal subluxation of the distal ulna and increased radial inclination are also observed. (i,j,k) Chest radiographs of individuals IV-1, IV-3 and IV-4 reveals normal rib and clavicular structure (l-n) Hand radiographs of all three affected siblings demonstrate severe brachydactyly. A V-shaped configuration of the proximal carpal row is also observed in the individual IV-3. (o-q) AP pelvic radiographs of the affected individuals (IV-1, IV-3 and IV-4) demonstrate bilateral coxa vara, and femoral bowing. (r-t) Lower limb radiographs of the individuals IV-1, IV-3 and IV-4 show shortened and broadened tibia and fibula with genu varum. Flared and irregular metaphyses of the distal femora and proximal tibiae, cortical thickening with narrowed medullary canals is noted. Multiple well-defined calcified loose bodies are seen in the left suprapatellar pouch and juxta-articular region in the affected individual IV-1. (u–v) Foot radiographs of the individuals IV-1, IV-4 depict short and broad tarsals, metatarsal, and phalangeal bones with bilateral fusion of the distal phalanges of the fifth toes. The distal metatarsal and proximal phalangeal epiphyses appear broad and squared. Fixed plantar flexion of the forefeet and equinus deformity at the ankle joints are also evident.

multiple well-defined calcified loose bodies were seen in the left suprapatellar pouch and juxtaarticular region (Figure 2r-t). The X-rays of the feet showed short and broad tarsals, metatarsals and phalangeal bones with bony fusion (synostosis) of the distal phalanges of the fifth toes bilaterally. The epiphyses, particularly of the distal metatarsals and proximal phalanges, appeared broad and slightly squared. There was evidence of fixed plantar flexion of the forefeet and equinus deformity at the ankle joints (Figure 2u, v) (Table 1).

All the patients of the family had normal intellect and central nervous system. Blood sugar levels, kidneys, heart and vision were normal. No central facial dysmorphic features were detected. Heterozygous carriers exhibited normal hands and feet with no other anomalies were noted.

Genetic findings

In the affected individual IV-1, WES analysis revealed a homozygous missense variant [(c.1018G>A; p. Val340Met) in the exon 3 of *IHH* gene, reporting the most significant variant. Segregation of the variant was tested using available DNA samples from the family members (III-7, IV-2, IV-3, IV-4) (Figure 3a). No homozygous occurrence of the variant was found in online population databases (EVC, ExAC, gnomAD, 1000genomes) or among 135 in-house Pakistani control exomes. Conservation analysis showed the wild type residue to be highly conserved among different species (Fig. 3B). The variant was estimated to be damaging and disease causing via different online software's: Mutation Taster, Versome, PolyPhen-2, Provean and SIFT FATHMM-MKL (Table 2). Based on ACMG criteria the sequence variant was classified as likely pathogenic (Table S1) [30].

Secondary and tertiary structure analysis and mutation outcomes

Understanding secondary structure elements is essential for acquiring deeper insights into the conformational changes at the 3D level. The Val340Met substitution occurs in the C-terminal auto processing domain of the IHH protein. The two-dimensional structural of IHH^{WT} comprised 10 β-sheets, a single helix, 10 beta turns and 4

Table 2. Pathogenicity of the identified variant (c.1018G>A; p. Val340Met)

S. No	Tool used	Prediction
1	Mutation Taster	Disease causing
2	SIFT	Damaging
3	Provean	Neutral
4	PolyPhen-2	Damaging
5	DANN	Disease causing (0.9986)
6	FATHMM-MKL	Damaging (Coding score 0.9894)
7	FATHMM	Damaging

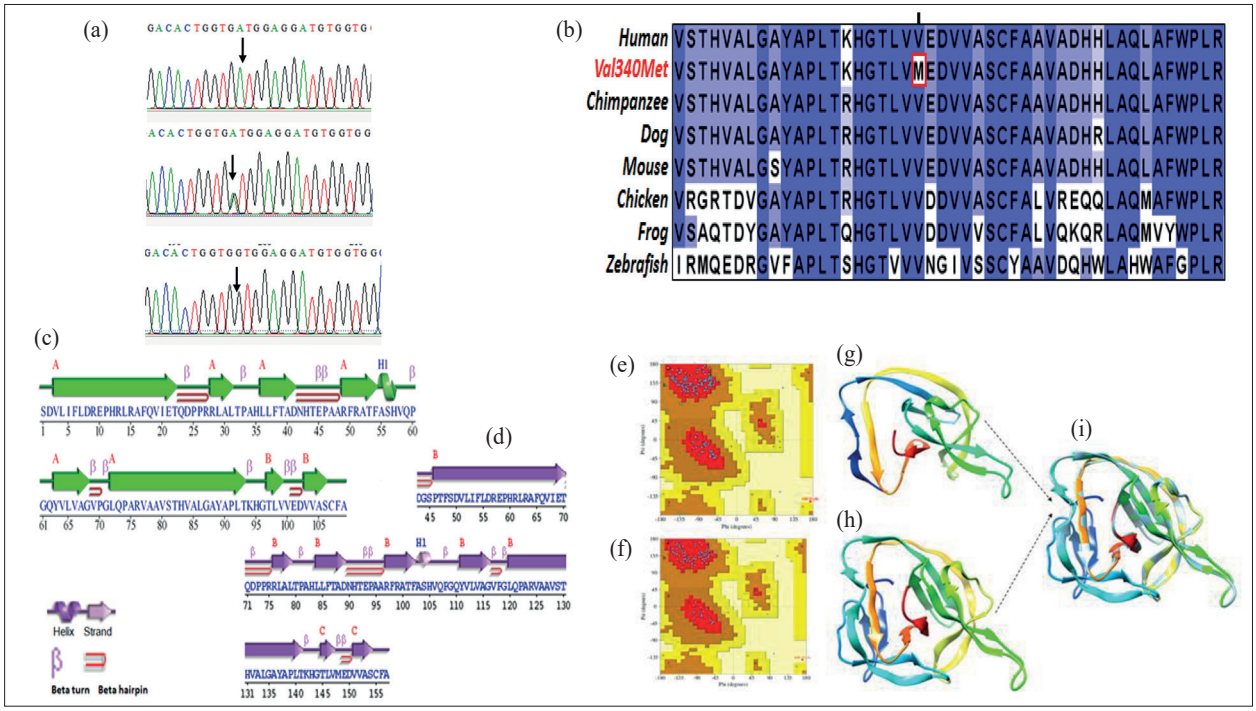

Figure 3. (a) Sanger electrograms of the variant (c.1018G>A; p. Val340Met) identified in an affected (upper panel), a carrier (middle panel) and a normal (lower panel) (b) Showing conservation of valine amino acid across several species. Secondary structure of (c)IHH^{WT} and (d) $IHH^{Val340Met.}$ Structure validation through Ramachandran plot (e) IHH^{WT} and (f) $IHH^{Val340Met}$ (g) and (h) represents ribbon form of wild type and mutant tertiary structures respectively. (i) Superimposition of mutant and wild type IHH auto processing domain.

Table S1. The sequence variant was classified as likely pathogenic based on ACMG criteria (Richards et al. 2015) [30]

Gene	*IHH*
Variant	c.1018G>A, p. Val340Met)
ACMG criteria pathogenic variant	
Strong	
PS1 - same AA as established pathogenic variant	
PS2 - denovo	
PS3 - *invitro* assay	
PS4 - increase prevalence of the variant	
Moderate	
PM1 - Mutational hotspot and/or critical and well-established functional domain	
PM3 - cis/trans with pathogenic variant	
PM4 - Protein length change	
PM5 - same aa position, different change	
PM6 - assumed denovo	
Supporting	
PM2 - absent from controls	✓
PP1 - cosegregation	✓
PP2 - low rate of benign missense variation	✓
PP3 - computaional evidence support	✓
PP4 - patient phenotypes highly specific	✓
PP5 - reputable resource reports as pathogenic	

hairpins loops. In contrast, IHH^{Val340Met}, exhibited changes in β-sheets lengths unlike RPTN^{WT} (Figure 3c and d).

To assess the structural impact of the identified mutation, wild type and mutant protein models of IHH (C-terminal auto processing domain) were generated and analysed. Ramachandran plots analysis of the modelled IHH^{WT} and IHH^{Val340Met} showed that over 95% residues were present in the sterically allowed region (Figure 3e, f, g and h). Both modelled structures displayed acceptable stereochemical quality with parameters including peptide bond planarity, non-bonded interactions, Cα tetrahedral distortion, main chain Hydrogen bond energy and G-factor within the favoured regions. Superimposition of IHH^{WT} and IHH^{Val340Met} produced an overall RMSD of Q score of 0.741(Figure 3i).

Due to their distinct chemical characteristics (hydrophobic versus amphipathic) and differences in side-chain size, the substitution of the wild-type valine residue with methionine may lead to several consequences. Firstly, the mutated residue lies within a domain critical for processing and secretion of the IHH protein and this substitution may disrupt interactions with binding partners thereby affect the function of the protein. Secondly the wild-type valine residue is buried within the protein core due to its hydrophobic nature, whereas the bulkier methionine side chain may not fit into protein core, disrupting the core packing and altering the overall protein conformation (Figure 4a and b).

The results of MDs were consistent with our structure analysis of the IHH protein. RMSF analysis derived from atom trajectories revealed high fluctuations in the region harbouring the p. Val340Met substitution (Figure

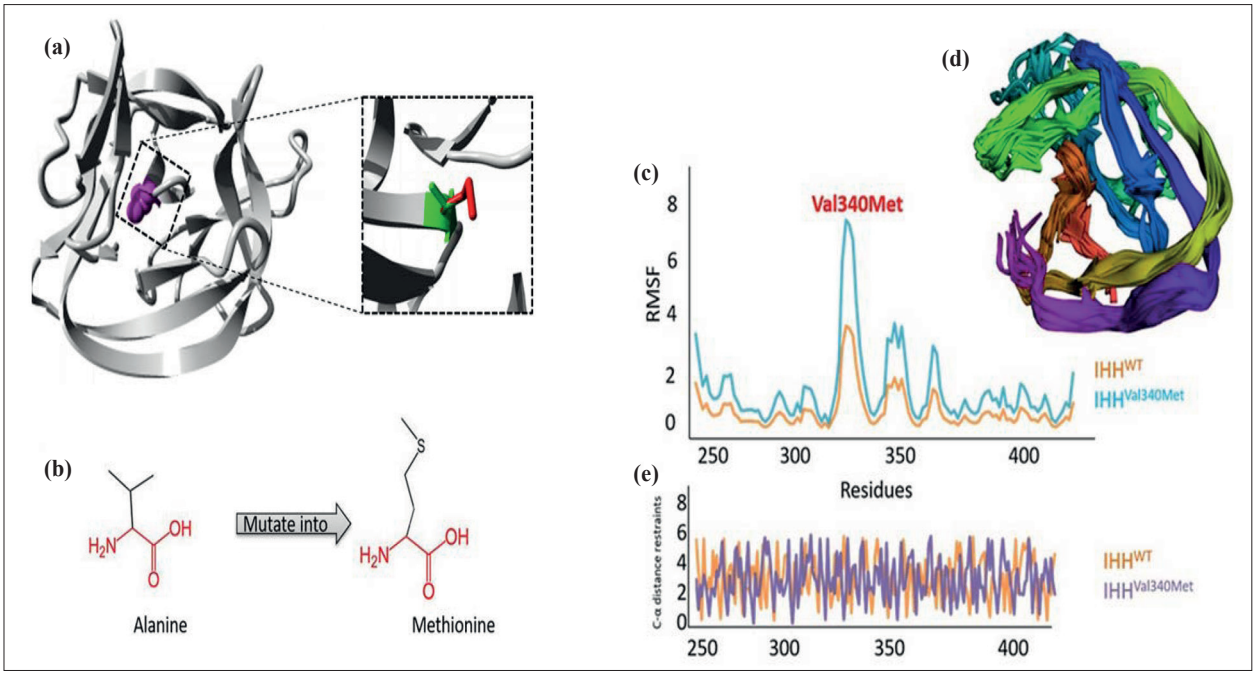

Figure 4. (a) Ribbon representation of protein in grey colour with mutant residue in magenta colour. In close up view side chain of both wild type and mutant residues are shown in green and red colour respectively. (b) schematic structures of the original (left) and the mutant (right) amino acid. The backbone, which is the same for each amino acid, is coloured red. The side chain, unique for each amino acid, is coloured black. RMSF analysis (c, d) simulation trajectories and (e) C-α distance restraints analysis.

4c and d) which was further validated by the C-α distance restraints analysis (Figure 4e). Simulations results suggests that p. Val340Met substitution resulted in loosely packed c-terminal auto processing domain of the IHH protein and significant structural alterations may contribute to protein dysfunction leading to disease onset. So, the identified substitution is thought to reduce the compactness and ultimately decrease the stability of the IHH protein.

DISCUSSION

The Hedgehog signaling pathway is a fundamental, evolutionarily conserved pathway required for skeletal development, particularly in coupling chondrogenesis with osteogenesis during endochondral ossification [31]. Among its three ligands—Sonic Hedgehog (SHH), Indian Hedgehog (IHH), and Desert Hedgehog (DHH)—IHH plays an important role in regulating chondrocyte proliferation and differentiation via the IHH–PTHrP feedback loop, ensuring growth plate maintenance [32]. IHH is mainly expressed by prehypertrophic and hypertrophic chondrocytes in the developing skeleton. Additionally, IHH directly promotes osteoblast differentiation in long bones through interactions with RUNX2 and BMPs, thus playing a central role in coordinating cartilage and bone development [33].

Mutations in *IHH* genes have been known to be linked to a range of skeletal chondrodysplasias, such as ACFD and brachydactyly type and mild disproportionate short stature [16,20-21]. Duplications of the *IHH* locus have also been associated with syndactyly and craniosynostosis [34].

In this study, we report a novel missense mutation (c.1018G>A, p. Val340Met) in a consanguineous Pakistani family with three affected individuals presenting with a novel form of AMDM like skeletal dysplasia via whole-exome sequencing. The identified mutation (p. Val340Met) was present in the C-terminal auto-processing domain that catalyses the cleavage of N- and C-terminal of the protein and facilitates the addition of a cholesterol molecule to the N-terminal signalling domain. The process of autocleavage and subsequent addition of the cholesterol molecule are thought to be important for both the secretion and sequestration of processed Hedgehog (HH) proteins [35]. Firstly, processed HH is recognised by a sterol recognition domain in Dispatched, a membrane protein thought to be responsible for transporting cholesterol-modified HH across the plasma membrane. Secondly, HH is recognised by a sterol recognition domain in Patched, a HH receptor and binds to it. In this way, extracellular HH is sequestered and the range of its effect is limited. The mutant Met amino acid being bigger compared to the wild type Val residue, may induce structural alterations in the protein core leading to a less compact C-terminal auto processing domain of the IHH protein. These potentially significant structural fluctuations may affect the function of the protein and cause disease onset, as shown by the structural analysis of the IHH Protein (Figure 3 and 4). Recent study by [36] supported the pathogenic relevance of variants in the IHH C-terminal domain, demonstrating that such mutations reduced the IHH secretion and ligand availability, leading to short stature and skeletal abnormalities.

Phenotypically the family presented a novel case of acromesomelic short stature that shares some similarities with AMDM and ACFD. Like both conditions, the affected members in the present family demonstrated disproportionate acromesomelic limb shortening, brachydactyly, clinodactyly and shortened femoral neck/shaft. While AMDM is frequently associated with kyphosis, lumbar lordosis and vertebral body changes, these were absent in our case. Furthermore, our patients displayed stable joints, taut and normal skin in contrast to the loose redundant skin and joint laxity reported in AMDM [13-14]. Radiographic evaluation of the forearms in our cohort demonstrated a classic Madelung deformity, characterized by volar and ulnar bowing of the distal radius, along with dorsal subluxation of the distal ulna, increased radial inclination, and V-shaped (triangular) configuration at the proximal carpal row. In contrast, AMDM is characterized by symmetrical shortening while in ACFD central epiphyseal coning is seen (Table 1).

Compared with ACFD, our patients demonstrated specific distal anomalies including synostosis of the distal phalanx of the fifth toe, fixed plantar flexion with equinus deformity, and metatarsus adductus, all of which were absent in ACFD [16]. In addition, hallmark radiographic features of ACFD (and AMDM) such as cone-shaped epiphyses and teardrop metacarpals were notably absent in our family as was narrow thorax and pectus deformities (Table 1).

The observed phenotypes in our study are also distinct from the GDF5-related AMDs (AMD2A-C). AMD2A is characterized by extreme limb shortening, rudimentary digits, loose and redundant skin whereas affected individuals in our case displayed normal digit count with preserved stable joints stability and taut skin. Furthermore, while AMD2B and AMD2C typically exhibits joint dislocations, straight normal bone structure and bone density, our family showed Madelung deformity with radial bowing and angulation along with hyperplastic distal femur and marked cortical sclerosis [6-8] (Table 1)

Although the core skeletal features including acromesomelic limb shortening, cortical sclerosis and Madelung-like deformity observed in our family were consistent in all three affected individuals (IV-1, IV-2, IV-4), intraarticular loose bodies were observed exclusively in the eldest af-

fected member (IV-1). X-rays of the left knee showed multiple, well-defined calcified loose bodies in the suprapatellar pouch and juxtaarticular region. These most likely representing a secondary degenerative process resulting from the dense hyperplasic structure of the distal femur and chronic joint malalignment.

Taken together, the combination of unique clinical findings and a novel pathogenic *IHH* variant points to a previously undescribed form of acromesomelic dysplasia. This report expands both the phenotypic and genotypic spectrum of IHH-related skeletal disorders and underscores the essential role of the IHH C-terminal domain in endochondral ossification.

DECLARATIONS

Author Contributions

Muhammad Hanif, Bashir Ahmad, Amir Hayat, Bushra Khan: Genetic studies, Clinical analysis and data analysis. Salman Hassan: Sampling; Nosheen Bibi: Performed the bioinformatics analysis; Umme Kalsoom, Siara Farman, Bushra Khan; Manuscript writing and revision: Bushra Khan: Design and conception of studies, supervision and coordination.

All authors have read and approved the final version of the manuscript.

Acknowledgments

The authors are highly thankful to the family members that participated in this study.

Funding

No funding was provided for the study

Competing interests

Authors declare no conflict of interest.

Ethics Approval

The research study was approved by Institutional Review Board (IRB), Abdul Wali Khan University Pakistan

Consent to participate

Informed written consent was taken from participating members of families. Blood sampling from unaffected and affected individuals were carried out according to guidelines provided by Declaration of Helsinki.

Data availability statement

We have submitted the novel variant to ClinVar (https://ncbi.nlm.nih.gov/clinvar/) under an accession number; SCV006277932 for IHH variant [(c.1018G>A, p. Val340Met)]

REFERENCE

1. Kurt F, Ceylaner S, Yakut HI (2013) Acromesomelic dysplasia with cardiac and neurologic abnormalities: An association by chance, new features of Maroteaux type or a new syndrome? Genet Counse 24: 75–80.
2. Khan S, Basit S, Khan MA, Muhammad N, Ahmad W (2016) Genetics of human isolated acromesomelic dysplasia. Eur J Med Genet 59: 198–203. https://doi.org/10.1016/j.ejmg.2016.02.011
3. Hassan M, & Lachman RS (2007) Taybi & Lachman's radiology of syndromes, metabolic disorders and skeletal dysplasias (5th ed.). Mosby.
4. Unger S, Ferreira CR, Mortier GR, Ali H, Bertola DR, Calder A, Cohn DH, Cormier-Daire V, Girisha KM, Hall C, Krakow D, Mäkitie O, Mundlos S, Nishimura G, Robertson SP, Savarirayan R, Sillence D, Simon M, Sutton VR, Superti-Furga A (2023) Nosology of genetic skeletal disorders: 2023 revision. Amer J Med Genet Part A 191: 1164–1209. https://doi.org/10.1002/ajmg.a.63132
5. Kant SG, Polinkovsky A, Mundlos S, Zabel B, Thomeer RTWM & Zonderland HM (1998) Acromesomelic dysplasia Maroteaux type maps to human chromosome 9. A J Hum Genet 63: 155–162. https://doi.org/10.1086/301917
6. Thomas JT, Kilpatrick MW, Lin,K, Erlacher L, Lembessis P, Costa T, Tsipouras P, Luyten, FP (1997) Disruption of human limb morphogenesis by a dominant negative mutation in CDMP1. Nature Genet 17: 58–64. https://doi.org/10.1038/ng0997-58
7. Faiyaz-Ul-Haque M, Ahmad W, Zaidi SHE, Haque S, Teebi AS, Ahmad M, Cohn DH, Tsui LC (2002) Mutation in the cartilage-derived morphogenetic protein-1 (CDMP1) gene in kindred affected with fibular hypoplasia and complex brachydactyly (Du Pan syndrome) Clin Genet 61: 454–458. https://doi.org/10.1034/j.1399-0004.2002.610610.x
8. Byrnes AM, Racacho L, Nikkel SM, Xiao F, MacDonald H, Underhill TM, Bulman DE (2010) Mutations in GDF5 presenting as semidominant brachydactyly A1. Hum Mut 31: 1155–1162. https://doi.org/10.1002/humu.21338
9. Stange K, Desir J, Kakar N, Mueller TD, Budde BS, Gordon CT, Horn D, Seemann P, Borck GA (2015) A hypomorphic BMPR1B mutation causes Du Pan acromesomelic dysplasia. Orphanet J Rare Dis10: 84. https://doi.org/10.1186/s13023-015-0299-5

10. Díaz-González F, Wadhwa S, Rodriguez-Zabala M, Kumar S, Aza-Carmona M, Sentchordi-Montane L, Alonso M, Ahmad I, Zahra S, Kumar D, Kushwah N, Shamim U, Sait H, Kapoor S, Roldan B, Nishimura G, Offiah AC, Faruq M, Heath KE (2022) Biallelic cGMP-dependent type II protein kinase gene (PRKG2) variants cause a novel acromesomelic dysplasia. J Med Genet 59: 28–38. https://doi.org/110.1136/jmedgenet-2020-107177
11. Osebold WR, Remondini DJ, Lester EL, Spranger JW, Opitz JM (1985) An autosomal dominant syndrome of short stature with mesomelic shortness of limbs, abnormal carpal and tarsal bones, hypoplastic middle phalanges, and bipartite calcanei. Am J Med Genet 22: 791–809. https://doi.org/10.1002/ajmg.1320220414
12. Faivre L, Le Merrer M, Megarbane A, Gilbert B, Mortier G, Cusin V, Munnich A, Maroteaux P, Cormier-Daire V (2000) Exclusion of chromosome 9 helps to identify mild variants of acromesomelic dysplasia Maroteaux type J Med Genet 37: 52–54. https://doi.org/10.1136/jmg.37.1.52
13. Wu J, Wang M, Jiao Z, Dou B, Li B, Zhang J, Zhang H, Sun Y, Tu X, Kong X, Bai Y (2022) Novel loss-of-function mutations in NPR2 cause acromesomelic dysplasia, Maroteaux type. Front Genet 13:823861. https://doi.org/10.3389/fgene.2022.823861
14. Bartels CF, Bukulmez H, Padayatti P, Rhee DK, van Ravenswaaij-Arts C, Pauli RM, Mundlos S, Chitayat D, Shih LY, Al-Gazali LI, Kant S, Cole T, Morton J, Cormier-Daire V, Faivre L, Lees M, Kirk J, Mortier GR, Leroy J, Zabel B, Kim CA, Crow Y, Braverman NE, van den Akker F, Warman ML (2004) Mutations in the transmembrane natriuretic peptide receptor NPR-B impair skeletal growth and cause acromesomelic dysplasia, type Maroteaux. Am J Hum Gen 75: 27–34. https://doi.org/10.1086/422013
15. Thomas JT, Lin K, Nandekar M, Camargo M, Cervenka J, Luyten FP (1996). A human chondrodysplasia due to a mutation in a TGF-beta superfamily member. Nature Genet. 12: 315-317. https://doi.org/10.1038/ng0396-315
16. Mortier GR, Kramer PPG, Giedion A, Beemer FA (2003) Acrocapitofemoral dysplasia: A newly recognized autosomal recessive skeletal dysplasia. J Med Genet 40: 201–207. https://doi.org/10.1136/jmg.40.3.201
17. Cubuk PO, Duz MB (2021) Acrocapitofemoral dysplasia: Novel mutation in IHH in two adult patients from the third family in the literature and progression of the disease. Eur J Med Genet 64: 104343. https://doi.org/10.1016/j.ejmg.2021.104343
18. Hellemans J, Coucke PJ, Giedion A, De Paepe A, Kramer P, Beemer F, Mortier GR (2003) Homozygous mutations in IHH cause acrocapitofemoral dysplasia, an autosomal recessive disorder with cone-shaped epiphyses in hands and hips. American Journal of Human Genetics 72:1040–1046. https://doi.org/10.1086/374318
19. Saeed T, Bibi N, Ahmad A, Khan S, Ansar M, Wasif N, Kalsoom U (2025) A novel biallelic variant in IHH causing acrocapitofemoral dysplasia in a Pakistani family. Mol Genet Genomic Med 13: e70085. https://doi.org/10.1002/mgg3.70085
20. Stattin EL, Lindén B, Lönnerholm T, Schuster J, Dahl N (2009) Brachydactyly type A1 associated with unusual radiological findings and a novel Arg158Cys mutation in the Indian hedgehog (IHH) gene. Eur J Med Genet 52(5): 297–302. https://doi.org/10.1016/j.ejmg.2009.05.008
21. Vasques GA, Funari MFA, Ferreira FM, Aza-Carmona M, Sentchordi-Montané L, Barraza-García J, Lerario AM, Yamamoto GL, Naslavsky MS, Duarte YA O, Bertola DR, Heath KE, Jorge AAL (2018) IHH gene mutations causing short stature with nonspecific skeletal abnormalities and response to growth hormone therapy. J Clin Endocrinol Metabol 103: 604–614. https://doi.org/10.1210/jc.2017-02026”
22. Yang J, Yan R, Roy A, Xu D, Poisson J, Zhang Y (2015) The I-TASSER suite: Protein structure and function prediction. Nature Methods 12: 7–8. https://doi.org/10.1038/nmeth.3213
23. Emsley P, Lohkamp B, Scott WG, Cowtan K (2010) Features and development of Coot. Acta Crystallographica Section D: Biological Crystallography, 66: 486–501. https://doi.org/10.1107/S0907444910007493
24. Gopalakrishnan K, Sowmiya G, Sheik SS, Sekar K (2007) Ramachandran plot on the web (2.0). Prot Peptid Lett 14: 669–671. https://doi.org/10.2174/092986607781483847
25. Laskowski RA, Rullmannn JA, MacArthur MW, Kaptein R, Thornton JM (1996) AQUA and PROCHECK-NMR: Programs for checking the quality of protein structures solved by NMR. J Biomol NMR 8: 477–486. https://doi.org/10.1007/BF00228148
26. Lüthy R, Bowie JU, Eisenberg D (1992) Assessment of protein models with three-dimensional profiles. Nature 356: 83–85. https://doi.org/10.1038/356083a0
27. Venselaar H, TeBeek TA, Kuipers RK, Hekkelman ML, Vriend G (2010) An e-science approach with life scientist friendly interfaces. BMC Bioinformat 11: 548. https://doi.org/10.1186/1471-2105-11-548

28. Duan Y, Wu C, Chowdhury S, Lee MC, Xiong G, Yang R, Cieplak P, Luo R, Lee T, Caldwell J, Wang, J, Kollman PA (2003) A point-charge force field for molecular mechanics simulations of proteins based on condensed-phase quantum mechanical calculations. Comput Chem 24: 1999–2012. https://doi.org/10.1002/jcc.10349
29. Zlenko DV (2012) Diffusion factor calculation for TIP4P model of water. Biofizika, 57:197–204. https://doi.org/10.1134/S0006350912020200
30. Richards S, Aziz N, Bale S et al (2015) Standards and guidelines for the interpretation of sequence variants: A joint consensus recommendation of the American College of Medical Genetics and Genomics and the Association for Molecular Pathology. Genet Med 17: 405–424. https://doi.org/10.1038/gim.2015.30
31. Chung UI, Schipani E, McMahon AP, Kronenberg HM (2001) Indian hedgehog couples chondrogenesis to osteogenesis in endochondral bone development. J Clin Invest 107: 295–304. https://doi.org/10.1172/JCI11706
32. Karp SJ, Schipani E, St-Jacques B, Hunzelman J, Kronenberg H, McMahon AP (2000) Indian hedgehog coordinates endochondral bone growth and morphogenesis via parathyroid hormone related-protein-dependent and -independent pathways. Development, 127: 543–548. https://doi.org/10.1242/dev.127.3.543
33. Long F, Chung UI, Ohba S, McMahon J, Kronenberg HM, McMahon AP (2004) Ihh signaling is directly required for the osteoblast lineage in the endochondral skeleton. Development 131: 1309–1318. https://doi.org/10.1242/dev.01006
34. Klopocki E, Lohan S, Brancati F, Koll R, Brehm A, Seemann P, Dathe K, Stricker S, Hecht J, Bosse K, Betz RC, Garaci FG, Dallapiccola B, Jain M, Muenke M, Ng VC, Chan W, Chan, D, Mundlos S (2011) Copy-number variations involving the IHH locus are associated with syndactyly and craniosynostosis. A J Hum Genet 88: 70–75. https://doi.org/10.1016/j.ajhg.2010.11.006
35. Burke R, Nellen D, Bellotto M, Hafen E, Senti KA, Dickson BJ, Basler K (1999) Dispatched, a novel sterol-sensing domain protein dedicated to the release of cholesterol-modified hedgehog from signalling cells. Cell 99: 803–815. https://doi.org/10.1016/S0092-8674(00)81677-3
36. Díaz-González F, Sentchordi-Montané L, Lucas-Castr E, Modamio-Høybjør S, Heath K E (2024) Variants in both the N- or C-terminal domains of IHH lead to defective secretion causing short stature and skeletal defects. Eur J Endocrinol 19: 38–46. https://doi.org/10.1093/ejendo/lvae072